A PFM-based Global Convergence Visual Servo Path Planner

ZHANG Xue-Bo[1] FANG Yong-Chun[1] MA Bo-Jun[1]

Abstract As a classical local path planning method, potential field method (PFM) is used widely in the robotics field because of its simplicity and elegance. However, a main drawback of this method is the existence of local minima when generating a path for a robot to follow. In this paper, we present a path planning approach for visual servo by using PFM method to keep the features within the camera field of view (FOV). A rigorous analysis is then presented to prove the global stability of the constructed path planning method. Moreover, the problem of how to obtain a better three-dimensional (3D) camera path is also studied extensively. Simulation results are provided to verify the performance of the proposed path planner.

Key words Potential field method (PFM), visual servo, field of view (FOV), global stability

During the past few years, the path planning problem has received considerable attention in the robotics field. It takes account of driving a robot from an initial configuration to the desired one by generating a path to follow. Currently, there are two main path planning approaches: global and local planning method. Global planning generally involves the construction and maintenance of a global map, and thus, heavy computing burden cannot be avoided. On the other hand, local planning methods such as potential field method (PFM) are much easier to implement and therefore, have gained increased popularity recently. Besides, PFM is an efficient way to enforce various external constraints for path planning of the robot because of its simplicity and elegance. Thus, it has been widely used for obstacle avoidance[1], mobile robot navigation[1−2], avoidance of joint limits[3−4], and so on. However, one main drawback of the local path planners is that the robot can be possibly trapped in local minima.

Recently, Mezouar and Chaumette extended PFM to generate a path in image space for visual servo[4−5]. Specifically, the potential field method was used to construct a two-dimensional (2D) image path, based on which the image-based visual servo algorithm was then used to enable a 6 degree-of-freedom (DOF) robot to track the generated path in image plane. This method is insensitive to the camera modeling errors because of the robustness of the image-based visual servo tracking algorithm. Moreover, features can be kept in the camera field of view (FOV) and other constraints such as joint limits and obstacle avoidance can be taken into account simultaneously. However, as a local path planner, the local minima problem is often met when generating the path using potential field method.

For visual servo purposes, a kernel problem is to ensure the FOV constraint during servo process. Many results have recently been reported on this issue. Unfortunately, most of the existing techniques usually lead to a long 3D trajectory of camera, which implies that the servo task might fail because of the limited workspace of the robot with joint limits, and that the servo efficiency is rather low, especially when the initial position of the camera is far away from its desired location. To solve this problem, some researchers tried to construct rotational and translational trajectories[6] similar to a circular motion to obtain a short 3D path for visual servo with large camera displacements by using adaptive control gains. However, to achieve high efficiency visual servo, it is preferred to obtain a straight line path instead of deriving a circular-like path in the presence of moderate camera displacements between the initial and desired locations. Motivated by that, [7] proposed a discontinuous method by switching among position-based control strategies and backward motion, so as a better 3D translational path is obtained and keep the features in FOV simultaneously. Unfortunately, position-based control strategies are often corrupted by image noise and camera modeling errors; moreover, this method requires 3D object model to be exactly known as a prior.

In this paper, an improved path planning approach for visual servo is proposed by using PFM method. By switching between attractive potential force and translational parts of the repulsive force, features can be kept in FOV and global stability can be achieved simultaneously. Besides, the problem of how to obtain a better 3D translational path is also studied extensively by allocating the weight of the six degrees of freedom in the repulsive potential force properly. First, some lemmas about the specific repulsive potential force are presented and then, used to prove the fact, that while planning the trajectory in 3D Cartesian space, local minima can be avoided by enforcing only translational parts of the repulsive force. By combining the idea of PFM with the inspiration to avoid local minima, a robust switching method for path planner is proposed to obtain the 3D&2D paths while ensuring the features in the camera field of view. Finally, to obtain a more efficient servo trajectory, the path planning approach is modified by introducing gain functions to adjust the weights for both translational and rotational part of the repulsive potential force. It should be noted that, by allocating gains properly, a better 3D camera path can be derived. This is important in practical view, because robots are mainly operated in limited work spaces. Besides, it should be pointed out that although 3D model is required to generate the path for the sake of concision, the planning method can be easily extended to unknown objects by combining it with the well-known homography decomposition technique[4−5].

The remaining part of this paper is organized as follows. Section 1 presents a robust switching path planner which ensures FOV constraint and global stability. To prove its performance, some lemmas and corresponding proofs are also included. Section 2 designs the gains allocation mechanism to obtain a better 3D camera path. Extensive simulation results are provided in Section 3 to verify the superior performance of the proposed approach. Finally, the conclusion is given in the last section.

Received July 19, 2007; in revised form November 21, 2007
Supported by Natural Science Foundation of Tianjin (07JCYBJC05400), Opening Project of National Laboratory of Industrial Control Technology of Zhejiang University (0708001), Program for New Century Excellent Talents in University (NCET-06-0210)
1. Institute of Robotics and Information Automatic System, Nankai University, Tianjin 300071, P. R. China
DOI: 10.3724/SP.J.1004.2008.01250

1 A switching path planner with global convergence

In the first part of this section, basic notation is provided and then, PFM for path planning in image space is reviewed briefly. In the second part, a switching path planner is proposed to guarantee global convergence and FOV constraint. In the third part, the performance of the path planner is analyzed with rigorous mathematical proofs.

1.1 Basic notation and PFM for visual path planning

Let O_c and O_d be the current and desired camera frame, and O_w be the world coordinate system. Then, consider a 3D stationary point lying in a reference plane π, and let $\boldsymbol{m}_c$, $\boldsymbol{m}_d$, and $\boldsymbol{m}_w$ denote its corresponding 3D coordinates expressed in O_c, O_d, and O_w, respectively. From simple geometry analysis, it is easy to obtain

$$\boldsymbol{m}_\sigma = {}^\sigma R_\kappa \boldsymbol{m}_\kappa + {}^\sigma \boldsymbol{t}_\kappa \tag{1}$$

where ${}^\sigma R_\kappa \in \mathbf{R}^{3\times 3}$ and ${}^\sigma \boldsymbol{t}_\kappa \in \mathbf{R}^3 (\sigma, \kappa \in \{w, c, d\})$ are the rotation matrix and translation vector between the frame O_κ and O_σ expressed in frame O_σ, respectively. Given the current and desired images, ${}^\sigma R_\kappa$ and ${}^\sigma \boldsymbol{t}_\kappa$ can be easily calculated using 3D pose estimation algorithm and the geometry constraint[4].

While planning the path, the configuration $\boldsymbol{\psi} = [{}^d \boldsymbol{t}_c^{\mathrm{T}}, (\boldsymbol{u}\theta)^{\mathrm{T}}]^{\mathrm{T}} \in \mathbf{R}^6$ is chosen to represent the 3D current pose of the camera, where $\boldsymbol{u} = [u_1, u_2, u_3]^{\mathrm{T}} \in \mathbf{R}^3$ and $\theta \in \mathbf{R}$ are the rotational axis and angle, respectively, that can be derived from the rotation matrix ${}^d R_c$ using Rodrigue′s formula[8−9]. Thus, when the camera is at the desired pose, the corresponding configuration $\boldsymbol{\psi}_d \in \mathbf{R}^6$ is $\boldsymbol{\psi}_d = \mathbf{0}$. Then, a discrete-time 3D trajectory is constructed from the current configuration $\boldsymbol{\psi}$ to the desired configuration $\boldsymbol{\psi}_d$ by the following transition equation[4−5]:

$$\boldsymbol{\psi}(k+1) = \boldsymbol{\psi}(k) + \frac{\varepsilon \cdot \boldsymbol{f}(k)}{\|\boldsymbol{f}(k)\|} \tag{2}$$

where $\varepsilon \in \mathbf{R}$ is a scalar representing the step size and $k \in \mathbf{R}$ denotes the current number of step, $\boldsymbol{f} \in \mathbf{R}^6$ is usually chosen as the linear combination of the potential forces with the following form:

$$\boldsymbol{f} = \boldsymbol{f}_a(\boldsymbol{\psi}) + \gamma \boldsymbol{f}_r(\boldsymbol{\psi}) \tag{3}$$

where $\gamma \in \mathbf{R}$ is a positive constant, and $\boldsymbol{f}_a(\boldsymbol{\psi})$ and $\boldsymbol{f}_r(\boldsymbol{\psi}) \in \mathbf{R}^6$ denote the attractive and repulsive force, respectively, which are defined as the negative gradient of the corresponding potential field.

1.2 A switching path planner design for visual servo

As illustrated by the subsequent simulation results, the path planning strategy of (3) often meets the local minimum problem, which means that robot might get trapped in a position other than the desired one. To solve this challenging problem, the following switching path planning method is designed by introducing gain functions:

$$\boldsymbol{f} = P\boldsymbol{f}_a + Q\boldsymbol{f}_r \tag{4}$$

where P, $Q \in \mathbf{R}^{6\times 6}$ are positive diagonal matrices, chosen as

$$P = g(\cdot) I_6 \tag{5}$$

$$Q = \begin{bmatrix} \vartheta_1(\cdot) I_3 & 0 \\ 0 & \vartheta_2(\cdot) I_3 \end{bmatrix} \tag{6}$$

where $g(\cdot), \vartheta_1(\cdot)$, and $\vartheta_2(\cdot) \in \mathbf{R}$ are all positive scalar functions, with $g(\cdot)$ used to represent the weight of the attractive force, whereas $\vartheta_1(\cdot)$ and $\vartheta_2(\cdot)$ are used to allocate the weights of the translational and rotational elements in the repulsive force, respectively.

Inspired by the idea of ensuring the FOV constraint and increasing servo efficiency, we use different path planning strategies for the cases of features lying in or outside the central area, and subsequently design a switching path planner as

$$\boldsymbol{f} = \begin{cases} P\boldsymbol{f}_a, & \text{when all features belong to area } C \\ Q\boldsymbol{f}_r, & \text{otherwise} \end{cases} \tag{7}$$

That is, when all the feature points lie in the central area, attractive force will take effect to steer the robot to its desired location; otherwise, when at least one feature point escapes out of the central area, repulsive force will be enforced to guarantee the visibility constraint. In (7), as is seen in Fig. 1, C is the central area of the image defined as[1]

$$C = \left\{ (u_i, v_i) | u_i \in (u_m + \alpha, u_M - \alpha) \cap v_i \in (v_m + \alpha, v_M - \alpha) \right\} \tag{8}$$

with u_m and u_M denoting the lower and upper bounds of the pixel coordinates along u axis, v_m and v_M are the corresponding bounds along the v axis. Inspired by the fact that local minimum can be avoided using only translational part of the repulsive force (refer to Section 1.3 for details), the gain functions are chosen as

$$g(\cdot) = \eta_1, \ \vartheta_1(\cdot) = \eta_2, \ \vartheta_2(\cdot) = 0 \tag{9}$$

in which η_1 and $\eta_2 \in \mathbf{R}$ are positive constants.

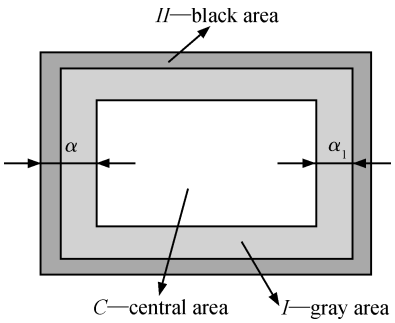

Fig. 1 The image boundary

In order to generate a straight line path while only the attractive force takes effect, the attractive potential force is generally defined as

$$\boldsymbol{f}_a(\boldsymbol{\psi}) = -\boldsymbol{\psi} \tag{10}$$

When the features are near the image boundary, we need to construct a virtual barrier to ensure the FOV constraint. In the existing techniques, all feature points should be considered in the repulsive field to make all the points move toward the center of the image[5]. However, it is actually not necessary to take into account the feature points in the central area C since they are practically not prone to escape from the image boundary. Based on this observation, a modified form of the repulsive potential field is constructed as

$$V_r(\boldsymbol{s}) = \sum_{i=1}^{n} V_r(\boldsymbol{s}_i) \tag{11}$$

[1]Other notations in Fig. 1 will be introduced in Section 1.4 for concision.

where

$$V_r(\boldsymbol{s}_i) = \begin{cases} 0, & \text{if } s_i \in C \\ \dfrac{1}{2}\ln\left(\dfrac{1}{(u_M - u_i)(u_m - u_i)(v_M - v_i)(v_m - v_i)}\right), & \text{otherwise} \end{cases} \tag{12}$$

In (11) and (12), $\boldsymbol{s} = [\boldsymbol{s}_1, \boldsymbol{s}_2, \cdots, \boldsymbol{s}_n] \in \mathbf{R}^{1\times 2n}$ consists of all the n feature points, and $\boldsymbol{s}_i = [u_i, v_i] \in \mathbf{R}^{1\times 2}(i = 1, 2, \cdots, n)$ is the 2D image coordinates of the i-th feature point. It should be noted that for every configuration of the feature points, different repulsive field is established, which is continuous both in and outside the central area C, and we further assume that the derivative of the repulsive field is zero on the boundary. Therefore, the repulsive potential force derived from $V_r(\boldsymbol{s})$ can be expressed as

$$\boldsymbol{f}_r(\boldsymbol{\psi}) = -\left(\frac{\partial V_r(\boldsymbol{s})}{\partial \boldsymbol{\psi}}\right)^{\mathrm{T}} = -M^{\mathrm{T}} L^{\mathrm{T}}(\boldsymbol{s}, \boldsymbol{Z}) \left(\frac{\partial V_r(\boldsymbol{s})}{\partial \boldsymbol{s}}\right)^{\mathrm{T}} \tag{13}$$

where $M \in \mathbf{R}^{6\times 6}$ is a coordinate transformation matrix that can be calculated as

$$M = \begin{bmatrix} {}^{d}R_c^{\mathrm{T}} & 0 \\ 0 & L_w^{-1}\,{}^{d}R_c^{\mathrm{T}} \end{bmatrix} \tag{14}$$

$$L_w^{-1} = I_3 + \frac{\theta}{2}\mathrm{sinc}\left(\frac{\theta}{2}\right) U_\times + (1 - \mathrm{sinc}(\theta))\, U_\times^2 \tag{15}$$

where $\mathrm{sinc}(\theta) = \sin(\theta)/\theta$, and $U_\times \in \mathbf{R}^{3\times 3}$ is referred to as the skew symmetric matrix derived from the vector $\boldsymbol{u}$. For n feature points, $P_1, P_2, \cdots, P_n$, $L(\boldsymbol{s}, \boldsymbol{Z}) \in \mathbf{R}^{2n\times 6}$ represents the image Jaccobian matrix (interaction matrix) derived as[8, 10]

$$L(\boldsymbol{s}, \boldsymbol{Z}) = \left[L(\boldsymbol{p}_1, Z_1)^{\mathrm{T}} \;\; L(\boldsymbol{p}_2, Z_2)^{\mathrm{T}} \;\; \cdots \;\; L(\boldsymbol{p}_n, Z_n)^{\mathrm{T}}\right]^{\mathrm{T}} \tag{16}$$

where

$$L(\boldsymbol{p}_i, Z_i) = \begin{bmatrix} -\dfrac{1}{Z_i} & 0 & \dfrac{x_i}{Z_i} & x_i y_i & -(1 + x_i^2) & y_i \\ 0 & -\dfrac{1}{Z_i} & \dfrac{y_i}{Z_i} & 1 + y_i^2 & -x_i y_i & -x_i \end{bmatrix} \tag{17}$$

with $\boldsymbol{m}_{ci} = [X_i, Y_i, Z_i]^{\mathrm{T}}$ denoting the 3D coordinates of the i-th point P_i expressed in O_c and $\boldsymbol{p}_i = [x_i, y_i]^{\mathrm{T}} = [X_i/Z_i, Y_i/Z_i]^{\mathrm{T}}$ being the normalized 2D image coordinates.

1.3 Performance analysis of the path planner

In this section, based on some reasonable assumptions, we introduce two lemmas and then, use them to prove the global convergence of the proposed switching path planner of (2), (7), and (9).

Assumption 1. The camera is always before the feature points, that is, $Z > 0$ for every 3D feature point $\boldsymbol{m} = [X, Y, Z]^{\mathrm{T}}$ expressed in the current camera frame O_c.

Assumption 2. The principal point of the camera intrinsic parameters is in the central area C defined in (8).

Assumption 3. All the feature points lie in the central area C in the desired image.

It should be noted that the above assumptions do not impose any requirements on the visual servo system. Assumption 1 is a standard one used frequently in visual servo control strategies[9, 11]. And Assumption 2 holds for almost all CCD cameras with feasible lens. Assumption 3 is generally a basic condition on the desired image to implement a robust visual servo task.

Let $f_{ri} \in \mathbf{R}$ be the i-th element of the repulsive force $\boldsymbol{f}_r$ derived in (13). Then f_{r3} is the repulsive force along the optical axis and it can be expressed as ${}^{c}f_{r3}$ in the current camera frame O_c.

Lemma 1. If at least one feature point lies outside area C, then, the repulsive potential force always drives the camera to move backward along the optical axis, that is,

$${}^{c}f_{r3} < 0 \tag{18}$$

Proof. Based on the repulsive potential field defined in (11) and (12), $\partial V_r(\boldsymbol{s})/\partial \boldsymbol{s}$ can be computed as

$$\frac{\partial V_r(\boldsymbol{s})}{\partial \boldsymbol{s}} = \left[\frac{\partial V_r(\boldsymbol{s})}{\partial \boldsymbol{s}_1} \;\; \frac{\partial V_r(\boldsymbol{s})}{\partial \boldsymbol{s}_2} \;\; \cdots \;\; \frac{\partial V_r(\boldsymbol{s})}{\partial \boldsymbol{s}_n}\right] \tag{19}$$

$$\frac{\partial V_r(\boldsymbol{s})}{\partial \boldsymbol{s}_i} = \begin{cases} (0\;0), & \text{if } s_i \in C \\ \begin{bmatrix} u_i - \dfrac{(u_M + u_m)}{2} & v_i - \dfrac{(v_M + v_m)}{2} \\ \dfrac{}{(u_M - u_i)(u_i - u_m)} & \dfrac{}{(v_M - v_i)(v_i - v_m)} \end{bmatrix}, & \text{otherwise} \end{cases} \tag{20}$$

where n denotes the number of the feature points, $i = 1, 2, \cdots n$.

After some mathematical manipulation by using (13), (16), (17), (19), and (20), we can obtain

$${}^{c}f_{r3} = -\sum_{i=1}^{m}\left(\frac{x_i\left(u_i - \dfrac{(u_M + u_m)}{2}\right)}{Z_i(u_M - u_i)(u_i - u_m)} + \frac{y_i\left(v_i - \dfrac{(v_M + v_m)}{2}\right)}{Z_i(v_M - v_i)(v_i - v_m)}\right) \tag{21}$$

where $m \in \mathbf{R}$ is the number of the feature points out of the central area C, and $[x_i, y_i]$ denote the normalized coordinates of the feature point expressed in the current camera frame O_c.

From Assumption 1, we know

$$Z_i > 0 \tag{22}$$

Using Assumption 2, we can derive the following inequality by the camera projection model

$$x_i\left(u_i - \frac{(u_M + u_m)}{2}\right) > 0,\;\; y_i\left(v_i - \frac{(v_M + v_m)}{2}\right) > 0 \tag{23}$$

Moreover, the following inequality holds for any feature points in the image

$$(u_M - u_i)(u_i - u_m) > 0,\;\; (v_M - v_i)(v_i - v_m) > 0 \tag{24}$$

By using (21)$\sim$(24), it is pretty straightforward to show

$${}^{c}f_{r3} < 0 \tag{25}$$

Therefore, the repulsive potential force always drives the camera to move backward along the optical axis. □

According to Lemma 1, the repulsive force will always drive the features back into the camera field of view. This is easy to understand in practice since all the feature points will move into the central area when the camera moves backward and far away from the feature points.

Lemma 2. If only translation ${}^d\boldsymbol{t}_c = [t_x, t_y, t_z]^{\mathrm{T}}$ exists between the current and the desired camera frame and $t_z < 0$, then at least one of the following two inequalities holds:

$$x_c t_x < 0 \quad \text{or} \quad y_c t_y < 0 \tag{26}$$

where $[x_c, y_c]$ is referred to as the normalized 2D image coordinates of any feature point outside the central area C in the current image.

Proof. Let $\boldsymbol{m}_d = [X_d, Y_d, Z_d]^{\mathrm{T}}$ denote the 3D coordinates of any feature point outside the central area C expressed in the desired camera frame. Then, its normalized 2D image coordinates can be written as

$$\begin{bmatrix} x_d \\ y_d \end{bmatrix} = \begin{bmatrix} \dfrac{X_d}{Z_d} \\ \dfrac{Y_d}{Z_d} \end{bmatrix} \tag{27}$$

Because only translation ${}^d\boldsymbol{t}_c = [t_x, t_y, t_z]^{\mathrm{T}}$ exists between the current and the desired camera frame, the 3D coordinate of this point $\boldsymbol{m}_c = [X_c, Y_c, Z_c]^{\mathrm{T}}$ in current camera frame O_c can be obtained

$$\begin{bmatrix} X_c \\ Y_c \\ Z_c \end{bmatrix} = \begin{bmatrix} X_d \\ Y_d \\ Z_d \end{bmatrix} - \begin{bmatrix} t_x \\ t_y \\ t_z \end{bmatrix} \tag{28}$$

Therefore, the corresponding normalized 2D coordinates in the current image frame can be easily obtained

$$\begin{bmatrix} x_c \\ y_c \end{bmatrix} = \begin{bmatrix} \dfrac{(X_d - t_x)}{(Z_d - t_z)} \\ \dfrac{(Y_d - t_y)}{(Z_d - t_z)} \end{bmatrix} \tag{29}$$

Since this feature point is currently outside central area C, while it lies in the area C in the desired image based on Assumption 3, the following facts can be proven

$$|x_c| > |x_d| \quad or \quad |y_c| > |y_d| \tag{30}$$

which then implies the following inequalities under Assumption 1 and the condition that $t_z < 0$

$$\begin{aligned} &|x_c| > |x_d| \Rightarrow \left|\frac{(X_d - t_x)}{(Z_d - t_z)}\right| > \left|\frac{X_d}{Z_d}\right| \Rightarrow \\ &|(X_d - t_x)| > |X_d| \Rightarrow t_x(X_d - t_x) < 0 \Rightarrow \\ &x_c t_x < 0 \\ &\text{or} \\ &|y_c| > |y_d| \Rightarrow y_c t_y < 0 \end{aligned}$$

□

Based on the above two lemmas, now, we are ready to show the performance of the designed path planner.

Theorem 1. Local minima can be avoided using the switching path planner proposed in Section 1.2. That is, the switching path planner of (2), (7), and (9) drives a robot to the desired pose without any local minima problem.

Proof. For the proposed switching path planner of (7), local minimum arises if and only if the following condition is satisfied near the boundary of central area C

$$\frac{P\boldsymbol{f}_a(k)}{\|P\boldsymbol{f}_a(k)\|} = -\frac{Q\boldsymbol{f}_r(k+1)}{\|Q\boldsymbol{f}_r(k+1)\|} \tag{31}$$

Case 1. If the rotation matrix between the current camera and the desired camera position ${}^dR_c \neq I_3$, obviously (31) cannot hold since the gains in (9) are chosen as $\vartheta_2(\cdot) = 0$.

Case 2. If ${}^dR_c = I_3$, then, $(\boldsymbol{u}\theta) = \boldsymbol{0}$ that is, only translation exists between the current and desired camera position. Thus, (31) is equivalent to the following equation by using (9), (10), (13), (14), (16), and (17):

$$\begin{bmatrix} t_x(k) \\ t_y(k) \\ t_z(k) \end{bmatrix} = -\frac{\eta_1\|P\boldsymbol{f}_a(k)\|}{\eta_2\|Q\boldsymbol{f}_r(k+1)\|} \begin{bmatrix} f_{r1}(k+1) \\ f_{r2}(k+1) \\ f_{r3}(k+1) \end{bmatrix} \tag{32}$$

where

$$\begin{bmatrix} f_{r1}(k+1) \\ f_{r2}(k+1) \\ f_{r3}(k+1) \end{bmatrix} = \begin{bmatrix} \displaystyle\sum_{i=1}^{m}\left(\frac{u_i - \dfrac{(u_M+u_m)}{2}}{Z_i(u_M-u_i)(u_i-u_m)}\right) \\ \displaystyle\sum_{i=1}^{m}\left(\frac{v_i - \dfrac{(v_M+v_m)}{2}}{Z_i(v_M-v_i)(v_i-v_m)}\right) \\ -\displaystyle\sum_{i=1}^{m}\left(\frac{x_i\left(u_i - \dfrac{(u_M+u_m)}{2}\right)}{Z_i(u_M-u_i)(u_i-u_m)} + \right. \\ \left. \dfrac{y_i\left(v_i - \dfrac{(v_M+v_m)}{2}\right)}{Z_i(v_M-v_i)(v_i-v_m)}\right) \end{bmatrix} \tag{33}$$

Therefore, to prove the fact that (31) never holds, it suffices to show that at least one element of the two sides of (32) has a different sign.

1) If $t_z \geq 0$, then based on lemma 1, we know that $f_{r3} < 0$, which obviously contradicts with the bottom equation of (32).

2) If $t_z < 0$, among the m feature points out of the central area C, define the sets N_1 and N_2 as

$$\begin{aligned} N_1 &= \{(u_i, v_i) | u_i < (u_m + \alpha) \cup u_i > (u_M - \alpha)\} \\ N_2 &= \{(u_i, v_i) | (u_m + \alpha) \leq u_i \leq (u_M - \alpha)\} \end{aligned}$$

where $i = 1, 2, \cdots, m$.

a) If more feature points lie in N_1 than in N_2. For each point (u_i, v_i) in N_1, by (21) and Lemma 2, we have

$$\frac{u_i - \dfrac{(u_M+u_m)}{2}}{Z_i(u_M-u_i)(u_i-u_m)} \cdot t_x < 0 \tag{34}$$

Besides, the repulsive force f_{r1} generated by a point (u_i, v_i) in N_1 is greater than that produced by a point (u_j, v_j) in N_2, since (u_i, v_i) is closer to the boundary along u axis, that is,

$$\left|\frac{u_i - \dfrac{(u_M+u_m)}{2}}{Z_i(u_M-u_i)(u_i-u_m)}\right| > \left|\frac{u_j - \dfrac{(u_M+u_m)}{2}}{Z_j(u_M-u_j)(u_j-u_m)}\right| \tag{35}$$

Therefore, because more feature points lie in N_1 than in N_2, (34) and (35) can be used to show

$$\sum_{i=1}^{m}\left(\frac{u_i-\dfrac{(u_M+u_m)}{2}}{Z_i(u_M-u_i)(u_i-u_m)}\right)\cdot t_x<0 \tag{36}$$

b) If more feature points lie in N_2 than in N_1, for a similar analysis, we have

$$\sum_{i=1}^{m}\left(\frac{v_i-\dfrac{(v_M+v_m)}{2}}{Z_i(v_M-v_i)(v_i-v_m)}\right)\cdot t_y<0 \tag{37}$$

It should be noted that when some features are out of the central area C of the current image, the sign of the elements in ${}^d\boldsymbol{t}_c$ keeps unchanged at the next step since the step size ε is rather small.

Therefore, with (36) and (37), we can prove that at least one element of ${}^d\boldsymbol{t}_c$ has a different sign with its corresponding element on the right-hand side of (32), thus, (31) never holds, which implies that local minima can be avoided and global stability is then guaranteed. □

1.4 A refined form of the path planner

Although the switching path planner proposed in (2), (7) and (9) ensures global convergence, a main drawback is that only translational elements of the repulsive force are used which implies a long 3D camera path when the initial and desired location are far apart. Besides, the chattering problem arises for the discontinuity of the switching path planner. Thus, suitable gain functions are introduced to alleviate the chattering problem and then, improve the performance of the path planner.

To facilitate later discussions, we split the image into three parts with C being the central area, I the outer, and II near the image edge (see Fig. 1 for details). The inspiration is that area I can be used to alleviate the discontinuity, and allocate the rotational and translational weights of the repulsive potential force properly to achieve a better 3D trajectory. Specifically, when the feature points are all in C, only the attractive force takes effect and thus, all the six elements of $\boldsymbol{\psi}$ decrease at the same rate; that is, 3D trajectory is the shortest — a straight line; otherwise, when at least one feature point enters I or II, both the attractive and repulsive force take effects. Moreover, the attractive force should decrease to zero gradually while the weight of repulsive force should increase when nearing II. Besides, to generate a better 3D camera path, rotation elements should take effect first to drive the features back into the central area and if it seems inefficient, the weight of the translational parts should be increased to ensure the FOV constraint. Finally, if at least one feature point enters II, then, only translational elements of the repulsive force take effect to keep the features in FOV and avoid the local minima simultaneously.

Based on the previous analysis, the path planner of (7) and (9) is refined as

$$\boldsymbol{f}=P\boldsymbol{f}_a+Q\boldsymbol{f}_r \tag{38}$$

where P, Q have been defined in (5), (6), and the gains are designed as

$$\eta(\cdot)=\max\{\Delta u,\Delta v\}/\alpha_1,\ g(\cdot)=\max\{c(1-\eta(\cdot)),0\} \tag{39}$$

$$\vartheta_1(\cdot)=\eta(\cdot)\exp\big(\lambda_1\eta(\cdot)\big),\ \vartheta_2(\cdot)=\eta(\cdot)\exp\big(-\lambda_2\eta(\cdot)\big) \tag{40}$$

with $\alpha_1\in\mathbf{R}$ being the width of I, and c, λ_1, $\lambda_2\in\mathbf{R}$ denoting positive constant, and Δu, $\Delta v\in\mathbf{R}$ representing the largest pixel distance of the feature points far away from the inner edge of I along the two image axes, respectively, that is,

$$\Delta u=\max\{\Delta u_1,\Delta u_2,\cdots,\Delta u_n\}$$
$$\Delta v=\max\{\Delta v_1,\Delta v_2,\cdots,\Delta v_n\}$$

where $\Delta u_i\ (i=1,2,\cdots,n)$ is defined as

$$\Delta u_i=\begin{cases}u_m+\alpha-u_i, & \text{if } u_i\le u_m+\alpha\\ 0, & \text{if } (u_m+\alpha)\le u_i\le(u_M-\alpha)\\ u_i-u_M+\alpha, & \text{if } u_i\ge u_M-\alpha\end{cases}$$

and $\Delta v_i\ (i=1,2,\cdots,n)$ is defined in the same way by substituting u by v.

2 Simulation results

In this section, extensive simulation results are provided to demonstrate the performance of the proposed path planner. In the first part, the global convergence is verified by the comparison with the common PFM method. The second part aims to demonstrate that FOV constraint is guaranteed and rather short 3D camera path can be obtained simultaneously.

2.1 Global convergence testing

When large pure rotation around the optical axis exists between the initial and desired position/orientation, local minimum arises for the common PFM-based path planner. In the following simulation, feature points are chosen as four vertices of a square, with its center being the origin of the world frame, in which z axis is perpendicular to the square. Besides, only translation along the optical axis exists between the camera and the world frame. In this case, the camera will move along and rotate around the optical axis driven by potential forces. The rotation and translation between the initial and desired pose are chosen as

$$\boldsymbol{u}=[0,\ 0,\ 1]^{\mathrm{T}},\ \theta=2.97\,\mathrm{rad},\ {}^d\boldsymbol{t}_c=\boldsymbol{0}$$

For the common PFM-based path planner (2) and (3), the gains are selected as

$$\varepsilon=0.001,\ \gamma=1$$

Fig. 2 (a) and (b) plot the translational and rotational errors between the current and desired location, respectively, from which we can see that both translation and rotation errors do not go to zero, and the robot, thus, gets trapped by a local minimum.

The corresponding results using the proposed path planner (2), (7), and (9) are shown in Fig. 3 (a), (b) with the gains selected as

$$\varepsilon=0.001,\ \eta_1=1,\ \eta_2=1$$

By using the proposed path planner, both translational and rotational errors go to zero ultimately. The actual performance consists of attractive force which drives the camera to its desired position and repulsive force which enforces the camera move backward to help decrease the rotational error, respectively.

2.2 FOV constraint and 3D camera path

To thoroughly testify the performance of the refined path planner of (2) and (38) ∼ (40), we provide the simulation results in presence of large rotation and translation with $\boldsymbol{u}, \theta$ and ${}^{d}\boldsymbol{t}_{c}$ chosen as

$$\boldsymbol{u} = [0.730\,3,\ -0.080\,4,\ -0.678\,4]^{\mathrm{T}},\ \theta = 2.08\,\mathrm{rad}$$
$${}^{d}\boldsymbol{t}_{c} = [105.8,\ 72.8,\ 78.8]^{\mathrm{T}}\,\mathrm{mm}$$

Wheaeas gain functions and constants of the refined path planner are selected as

$$\varepsilon = 0.02,\ c = 10,\ \lambda_1 = 4,\ \lambda_2 = 4$$

The result of the 2D image paths are presented by the solid lines in Fig. 4 (a), where the four points connected by dot-dash lines represent 2D positions of the feature points

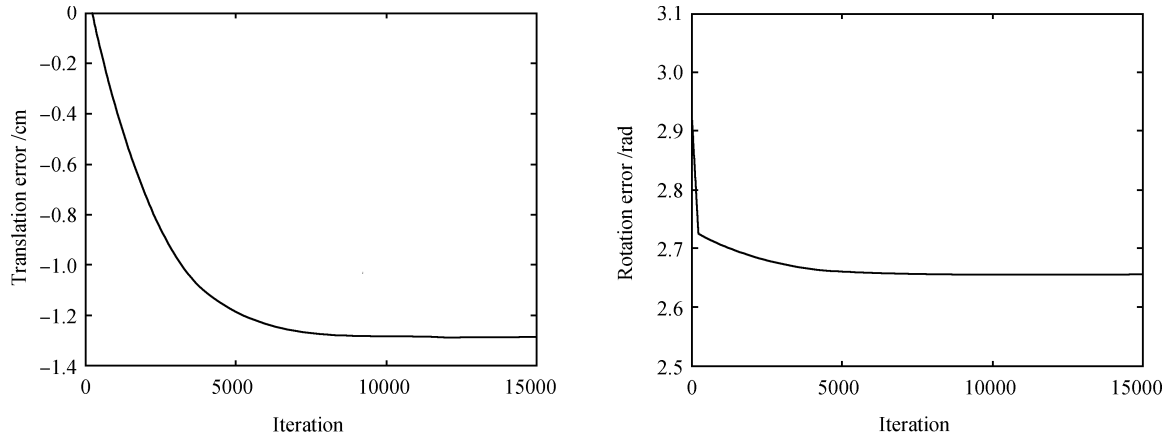

(a) Translation error along the optical axis (b) Rotation error around the optical axis

Fig. 2 Performance of the common path planner in presence of pure rotation

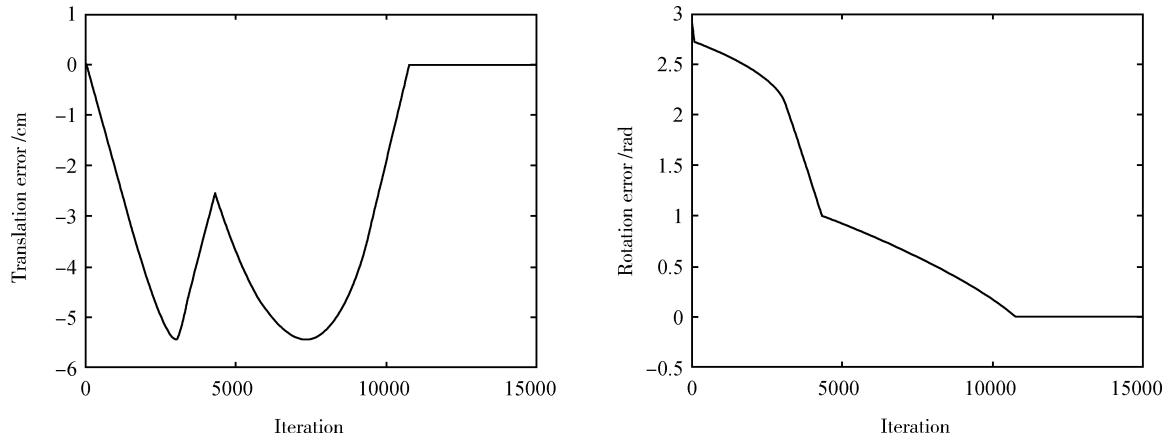

(a) Translation error along the optical axis (b) Rotation error around the optical axis

Fig. 3 Performance of the proposed path planner in presence of pure rotation

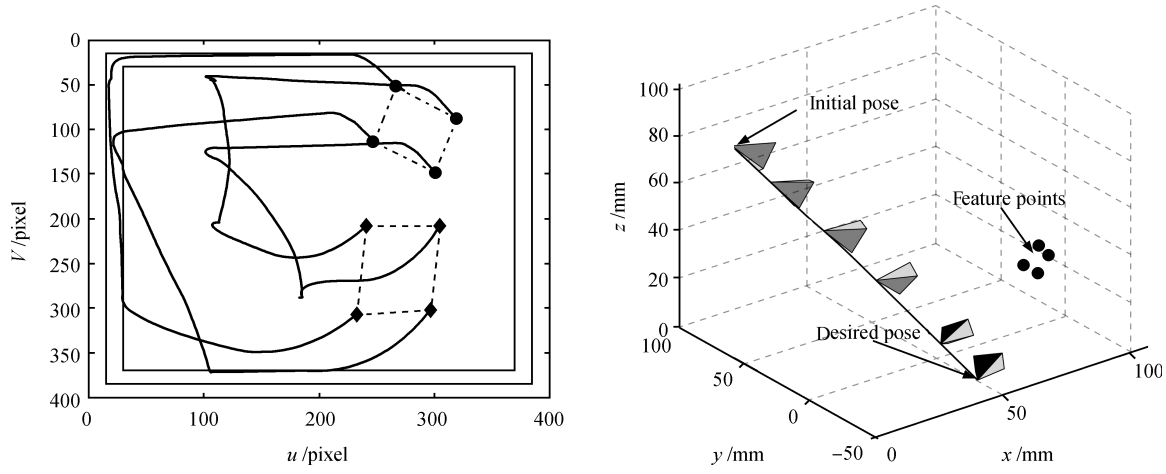

(a) 2D image paths of the feature points (b) The 3D camera path

Fig. 4 2D & 3D paths when rotation is large

in the initial image while the points connected by dash lines denote the ones in the desired image. From this figure, we can see that during the planning process, features are kept in the field of view consistently in the presence of large rotation and translation. The planned 3D camera path is depicted in Fig. 4 (b) with the pentahedrons representing several positions of the simulated camera, in which a rather short path (almost a straight line) is obtained. Therefore, the path planner successfully solves the potential failure problem for visual servo because of features out of FOV and increases the servo efficiency in the presence of limited operating space.

3 Conclusions

The paper constructs an elegant PFM-based visual servo path planner which ensures global convergence and guarantees the FOV constraint simultaneously. The performance of the proposed path planner is demonstrated by both theoretical analysis and simulation results. The path planner algorithm is further refined to obtain a better path so that higher servo efficiency can be achieved. Future work will focus on transforming the planned visual path into an admissible trajectory for the robot manipulators to track by using visual servo algorithms. Another interest is to extend the visual path planning method for nonholonomic mobile robots.

References

1 Ratering S, Gini M. Robot navigation in a known environment with unknown moving obstacles. In: Proceedings of IEEE International Conference on Robotics and Automation. Atlanta, USA: IEEE, 1993. 25−30

2 Shimoda S, Kuroda Y, Iagnemma K. Potential field navigation of high speed unmanned ground vehicles on uneven terrain. In: Proceedings of IEEE International Conference on Robotics and Automation. Barcelona, Spain: IEEE, 2005. 2828−2833

3 Marchand E, Hager G D. Dynamic sensor planning in visual servoing. In: Proceedings of IEEE International Conference on Robotics and Automation. Leuven, Belgium: IEEE, 1998. 1988−1993

4 Mezouar Y, Chaumette F. Path planning for robust image-based control. *IEEE Transactions on Robotics and Automation*, 2002, **18**(4): 534−549

5 Mezouar Y, Chaumette F. Path planning in image space for robust visual servoing. In: Proceedings of IEEE International Conference on Robotics and Automation. San Francisco, USA: IEEE, 2000. 2759−2764

6 Chesi G, Vicino A. Visual servoing for large camera displacements. *IEEE Transactions on Robotics*, 2004, **20**(4): 724−735

7 Chesi G, Hashimoto K, Prattichizzo D, Vicino A. Keeping features in the field of view in eye-in-hand visual servoing: a switching approach. *IEEE Transactions on Robotics*, 2004, **20**(5): 908−914

8 Chaumette F, Hutchinson S. Visual servo control part II: advanced approaches. *IEEE Robotics and Automation Magazine*, 2007, **14**(1): 109−118

9 Malis E, Chaumette F, Boudet S. 2-1/2-D visual servoing. *IEEE Transactions on Robotics and Automation*, 1999, **15**(2): 238−250

10 Chaumette F. *Potential Problems of Stability and Convergence in Image-based and Position-based Visual Servoing*. Berlin: Springer-Verlag, 1998. 66−78

11 Fang Y C, Dixon W E, Dawson D M, Chawda P. Homography-based visual servo regulation of mobile robots. *IEEE Transactions on Systems, Man, and Cybernetics, Part B: Cybernetics*, 2005, **35**(5): 1041−1050

ZHANG Xue-Bo Ph. D. candidate at the Institute of Robotics and Information Automatic System (IRIAS), Nankai University. He received his B. S. degree in automation from Tianjin University in 2006. His research interest covers visual servo control, mobile robot, and computer vision. E-mail: zhangxb@robot.nankai.edu.cn

FANG Yong-Chun Received his B. S. degree in electrical engineering and M. S. degree in control theory and applications from Zhejiang University in 1996 and 1999, respectively, and Ph. D degree in electrical engineering at Clemson University, USA, in 2002. From 2002 to 2003, he was a postdoctoral fellow at the Mechanical and Aerospace Engineering Department, Cornell University. He is currently a professor at the Institute of Robotics and Information Automatic System (IRIAS), Nankai University. His research interest covers nonlinear control, visual servoing, and control of underactuated systems including overhead cranes. Corresponding author of this paper.
E-mail: yfang@robot.nankai.edu.cn

MA Bo-Jun Ph. D. candidate at the Institute of Robotics and Information Automatic System (IRIAS), Nankai University. He received his B. S. degree in automation from Nankai University in 2004. His research interest covers nonlinear control, robotics, and computer vision.
Email: mabj@robot.nankai.edu.cn